A STUDY OF KC-135 AIRCRAFT ANTENNA PATTERNS

W.D. Burnside, R.J. Marhefka, C.L. Yu

The Ohio State University

ElectroScience Laboratory

Department of Electrical Engineering
Columbus, Ohio 43212

Technical Report 3001-9

Grant NGR 36-008-144

March 1974

National Aeronautics and Space Administration
Langley Research Center
Hampton, VA 23665

NOTICES

When Government drawings, specifications, or other data are used for any purpose other than in connection with a definitely related Government procurement operation, the United States Government thereby incurs no responsibility nor any obligation whatsoever, and the fact that the Government may have formulated, furnished, or in any way supplied the said drawings, specifications, or other data, is not to be regarded by implication or otherwise as in any manner licensing the holder or any other person or corporation, or conveying any rights or permission to manufacture, use, or sell any patented invention that may in any way be related thereto.

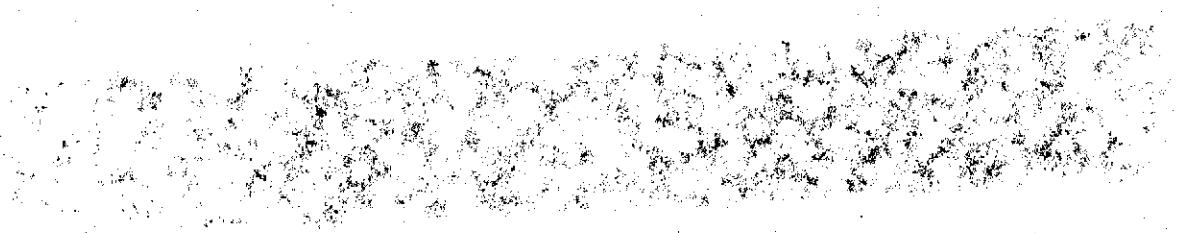

A STUDY OF KC-135 AIRCRAFT ANTENNA PATTERNS

W.D. Burnside, R.J. Marhefka, C.L. Yu

Technical Report 3001-9

Grant NGR 36-008-144

March 1974

National Aeronautics and Space Administration
Langley Research Center
Hampton VA 23365

ABSTRACT

Numerical solutions for the radiation patterns of aircraft antennas provide an excellent means of designing and locating antennas in order to achieve the desired performance. The high frequency solutions presented in this report are based on fuselage antennas mounted on a general-type aircraft but applied specifically to the KC-135 aircraft. The roll and elevation plane patterns are computed for a monopole, axial slot, and circumferential slot mounted both over and forward of the wings. In each case the calculated patterns compare very favorably with the measured patterns. The precision pattern measurements were taken on a 1/25 scale model of the KC-135 aircraft at NASA (Langley, Virginia) with special emphasis on reducing the mount and background effects.

TABLE OF CONTENTS

		Page
I.	INTRODUCTION	1
II.	DIFFRACTION BY ELLIPTIC CYLINDER	1
	A. Monopole Case	2
	B. Slot Case	3
III.	SCALE MODEL MEASUREMENTS	7
IV.	ELEVATION PLANE RADIATION PATTERN	7
V.	ROLL PLANE ANALYSIS	9
VI.	CONCLUSIONS	18
REFERENCES		19

I. INTRODUCTION

The need for an analysis of on-aircraft antenna patterns is quite apparent. If modern systems are to function properly, the antenna pattern must meet certain specifications. In fact, system performance is very much dependent upon the resulting patterns. In most cases, scale model measurements have been used to design and locate antennas. However, this approach is both expensive and time consuming. To alleviate this situation, it is proposed that theoretical solutions can be used very efficiently and accurately to predict certain antenna patterns. Using this approach one can evaluate an antenna's performance without having to build large numbers of scale models and spending a great deal of time mounting antennas and measuring their patterns.

The approach applied for these solutions is the Geometrical Theory of Diffraction (GTD). It is a high frequency technique with the only limitation being that the source and various scattering centers be separated on the order of a wavelength or more. In some cases even this requirement can be relaxed. With this restriction our lower frequency limit is around 100 MHz. The upper frequency limit is dependent on how well the theoretical model simulates the actual structure.

This paper is specifically concerned with computing the elevation and roll plane patterns for antennas mounted on a KC-135 (Boeing 707) aircraft. The elevation plane pattern is computed using a two-dimensional composite elliptic structure. The two-dimensional structure is valid in that the object is large electrically and the dominant terms are represented in this model as verified by a comparison with measured data. The roll plane pattern is computed using an elliptic cylinder fuselage model to which flat plate wings are attached. Again the agreement between calculated and measured results is very good.

II. DIFFRACTION BY ELLIPTIC CYLINDER

The radiation from slots and monopoles mounted on smooth curved surfaces is pertinent to the design of flush-mounted antennas for aircraft and spacecraft. Recently, Pathak and Kouyoumjian[1] have extended the GTD technique for plane wave diffraction by perfectly conducting convex surfaces to treat the radiation problem. This extension of GTD has been successfully applied to circular and elliptic cylinders, spheres, and spheroids[2].

The GTD solutions for the radiated electric field of infinitesimal slot and monopole antennas mounted on an elliptic cylinder as shown in Fig. 1 are given, neglecting torsional effects, by [1,2,3]

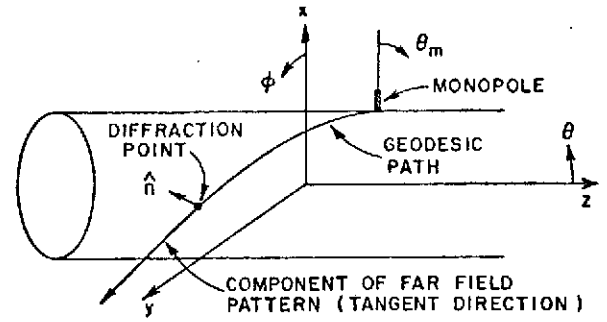

(a) GEOMETRY OF MONOPOLE PROBLEM

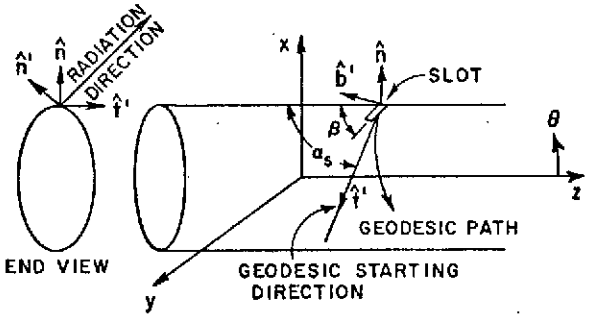

(b) GEOMETRY OF SLOT PROBLEM

Fig. 1. Geometry of antennas mounted on an infinitely long elliptic cylinder.

A. Monopole Case

Lit Region

(1) $$\vec{E} = -\sin\theta_m\,\hat{\theta}_m\,F(\text{source})$$

Transition Region

a) Lit side

(2) $$\vec{E} = \hat{n}\left\{(\sin\theta_m)1/2\; e^{jk\ell}\; g^*\left[-\int\left(\frac{k}{2\rho_g^2(\ell)}\right)^{1/3} d\ell\right]\right\}\cdot F(\text{tangent})$$

b) Shadow side

(3) $$\vec{E} = \hat{n}\left\{1/2\;\sqrt{\frac{d\psi_o}{d\psi}}\; e^{-jk\ell}\; g^*\left[\int\left(\frac{k}{2\rho_g^2(\ell)}\right)^{1/3} d\ell\right]\right\}\cdot F(\text{tangent})$$

Deep Shadow Region

(4) $$\vec{E} = \sum_j \hat{n}_j \, E_j^h \, F_j \text{ (tangent)}$$

B. Slot Case

Lit Region

(5) $$\vec{E} = [(\hat{e}_1 \sin\beta - \hat{e}_2 \cos\beta) \cdot (\hat{b}'\hat{n}' + \hat{t}'\hat{b}'\cos\theta_m)] \cdot F(\text{source})$$

Transition Region

a) Lit side

(6) $$\vec{E} = \left\{ \hat{n} \left[1/2 \, e^{jk\ell} \, g^* \left(- \int \left(\frac{k}{2\rho_g^2(\ell)} \right)^{1/3} d\ell \right) \sin(\alpha_s + \beta) \right] + \right.$$

$$\left. \hat{b} \left[j/2 \, e^{jk\ell} \, g^* \left(- \int \left(\frac{k}{2\rho_g^2(\ell)} \right)^{1/3} d\ell \right) \left(\frac{2}{k\rho_g} \right)^{1/3}_{\text{at source}} \cos(\alpha_s + \beta) \right] \right\}$$

$$\cdot \, F(\text{tangent})$$

b) Shadow side

(7) $$\vec{E} = \left\{ \hat{n} \left[1/2 \, \frac{d\psi_o}{d\psi} \, e^{-jk\ell} \, g^* \left(\int \left(\frac{k}{2\rho_g^2(\ell)} \right)^{1/3} d\ell \right) \sin(\alpha_s - \beta) \right] + \right.$$

$$\left. \hat{b} \left[- j/2 \, \frac{d\psi_o}{d\psi} \, e^{-jk\ell} \, g^* \left(\int \left(\frac{k}{2\rho_g^2(\ell)} \right)^{1/3} d\ell \right) \left(\frac{2}{k\rho_g} \right)^{1/3}_{\text{at source}} \cos(\alpha_s - \beta) \right] \right\}$$

$$\cdot \, F(\text{tangent})$$

Deep Shadow Region

$$\vec{E} = \sum_j \left[\hat{n}_j \, E_j^h \sin(\alpha_s - \beta) + \hat{b}_j \, E_j^s \cos(\alpha_s - \beta) \right] F_j(\text{tangent}) \tag{8}$$

where

$$E^h = \sqrt{\frac{d\psi_o}{d\psi}} \sum_{m=0}^{1} D_m^h \, L_m^h \, e^{-\int \gamma_m^h(\ell) d\ell}$$

$$E^s = \sqrt{\frac{d\psi_o}{d\psi}} \sum_{m=0}^{1} D_m^s \, L_m^s \, e^{-\int \gamma_m^s(\ell) d\ell}$$

$g^*(\ )$, $\tilde{g}^*(\ )$ = complex conjugates of the Fock functions[1].

$\hat{n}$, $\hat{b}$, $\hat{t}$ = the normal, binormal, and tangent unit vectors to the surface.

$F(\ )$ = phase factor to refer the phase to the center of the coordinate system.

$\sqrt{d\psi_o/d\psi}$ = is the spread factor and equals unity for this case[1].

ρ_g, ρ_t = longitudinal and transverse radii of curvature.

Note that the superscripts h and s indicate the hard and soft boundary conditions, respectively. The launch coefficients are given by [1]

$$L_m^h = \left[\pi e^{j\frac{\pi}{12}} D_m^h \left(\frac{2}{k\rho_g} \right)^{1/3} A_i(-\bar{q}_m) \right] \text{ at the source}$$

$$L_m^s = \left[\pi e^{-j\frac{\pi}{12}} D_m^s \left(\frac{2}{k\rho_g} \right)^{2/3} A_i'(-q_m) \right] \text{ at the source}$$

where D_m is defined in Table I. The subscript m refers to the mth mode of the boundary layer surface wave. Thus, γ_m is the propagation constant

TABLE I

GENERALIZED DIFFRACTION COEFFICIENTS AND ATTENUATION CONSTANTS

Surface	Square of Diffraction Coefficient D_m^2 = (Column A) · (Column B)		Attenuation Constant α_m = (Column C) · (Column D)	
	A. Keller's Result	B. Correction Terms	C. Keller's Result	D. Correction Terms
Soft Acoustic and Soft EM	$\frac{\pi^{-1/2}2^{-5/6}\rho_g^{1/3}e^{-j\pi/12}}{k^{1/6}A_i'(-q_m)^2}$	$1+\left(\frac{2}{k\rho_g}\right)^{2/3} q_m\left(\frac{1}{30}+\frac{\rho_g}{4\rho_{tn}}+\frac{\rho_g\bar{\rho}_g}{180}\right)e^{-j\pi/3}$	$\frac{q_m}{\rho_g}e^{j\pi/6}\left(\frac{k\rho_g}{2}\right)^{1/3}$	$1+\left(\frac{2}{k\rho_g}\right)^{2/3} q_m\left(\frac{1}{60}-\frac{2}{45}\rho_g\bar{\rho}_g+\frac{4}{135}\dot{\rho}_g^2\right)e^{-j\pi/3}$
Hard Acoustic	$\frac{\pi^{-1/2}2^{-5/6}\rho_g^{1/3}e^{-j\pi/12}}{k^{1/6}\bar{q}_m(Ai(\bar{q}_m))^2}$	$1+\left(\frac{2}{k\rho_g}\right)^{2/3}\left(\bar{q}_m\left(\frac{1}{30}+\frac{\rho_g}{4\rho_{tn}}+\frac{\rho_g\bar{\rho}_g}{180}\right)-\frac{1}{\bar{q}_m^2}\left(\frac{1}{10}+\frac{\rho_g}{4\rho_{tn}}-\frac{\rho_g\bar{\rho}_g}{60}\right)\right)e^{-j\pi/3}$	$\frac{\bar{q}_m}{\rho_g}e^{j\pi/6}\left(\frac{k\rho_g}{2}\right)^{1/3}$	$1+\left(\frac{2}{k\rho_g}\right)^{2/3}\left(\bar{q}_m\frac{1}{60}-\frac{2}{45}\rho_g\bar{\rho}_g+\frac{4}{135}\dot{\rho}_g^2\right)+\frac{1}{\bar{q}_m^2}\left(\frac{1}{10}+\frac{\rho_g}{4\rho_{tn}}-\frac{\rho_g\bar{\rho}_g}{60}+\frac{\dot{\rho}_g^2}{90}\right)\Big)e^{-j\pi/3}$
Hard EM		$1+\left(\frac{2}{k\rho_g}\right)^{2/3}\left(\bar{q}_m\left(\frac{1}{30}+\frac{\rho_g}{4\rho_{tn}}+\frac{\rho_g\bar{\rho}_g}{180}\right)-\frac{1}{\bar{q}_m^2}\left(\frac{1}{10}-\frac{\rho_g}{4\rho_{tn}}-\frac{\rho_g\bar{\rho}_g}{60}\right)\right)e^{-j\pi/3}$		$1+\left(\frac{2}{k\rho_g}\right)^{2/3}\left(\bar{q}_m\left(\frac{1}{60}-\frac{2}{45}\rho_g\bar{\rho}_g+\frac{4}{135}\dot{\rho}_g^2\right)+\frac{1}{\bar{q}_m^2}\left(\frac{1}{10}-\frac{\rho_g}{4\rho_{tn}}-\frac{\rho_g\bar{\rho}_g}{60}+\frac{\dot{\rho}_g^2}{90}\right)\Big)e^{-j\pi/3}$

for the mth mode surface wave such that $\gamma_m = \alpha_m + jk$ where α_m is defined in Table I. The incremental arc length along the geodesic path is expressed by $d\ell$. The summation over "j" in the shadow region indicates that several terms can contribute in that region.

One must first find an efficient solution for the geodesic paths on the elliptic cylinder surface in order to analyze this problem successfully using GTD. A preferred coordinate system for the elliptic cylinder is illustrated in Fig. 2 and defined by

$$\begin{aligned} x &= d \cosh u \cos v = a_f \cos v \\ y &= d \sinh u \sin v = b_f \sin v \\ z &= z \end{aligned} \tag{9}$$

where 2d is the distance between the foci of the ellipse. Note that for $u = u_f$, where $u_f = \tanh^{-1}(b_f/a_f)$, the above equations define an elliptical surface for $0 \le v < 2\pi$. Thus, the general shape of the elliptic surface is expressed by u_f, and its dimensions are defined by d.

Using the calculus of variations, the geodesic paths on an elliptical surface are given by

$$z = \frac{C}{\sqrt{1-C^2}} \int_{v_i}^{v_f} \sqrt{a_f^2 \sin^2 v + b_f^2 \cos^2 v}\, dv \quad . \tag{10}$$

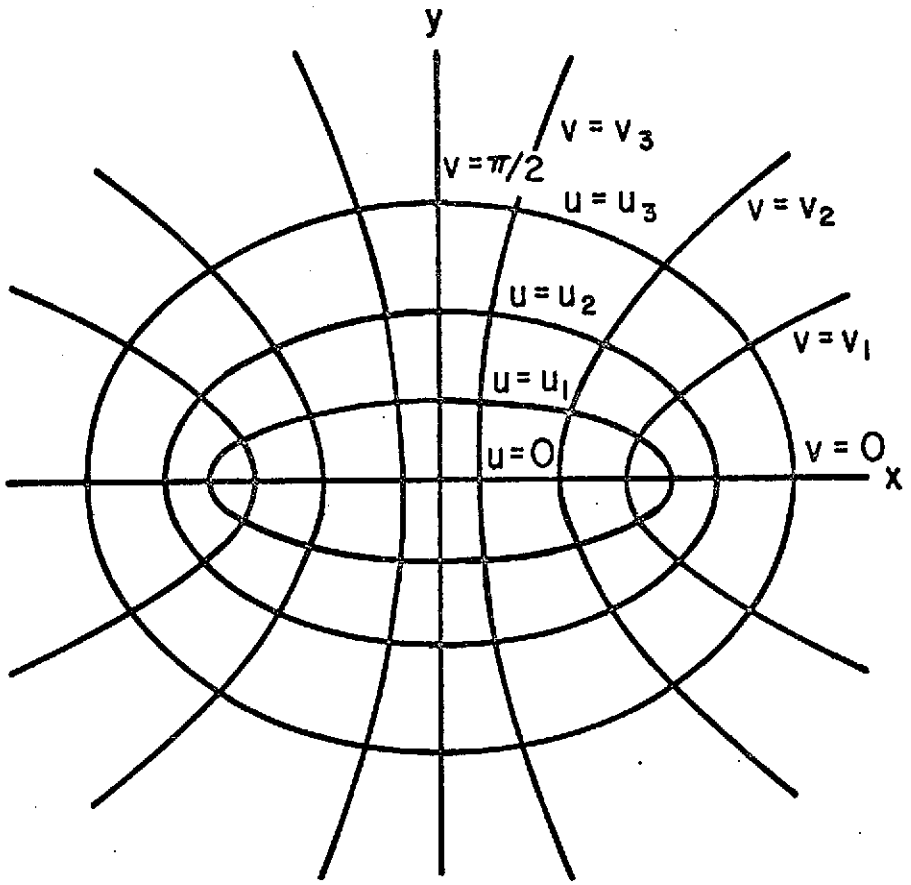

Fig. 2. Diagram showing the elliptic cylinder coordinate system.

Note that v_i and v_f are, respectively, the initial and final values of v along a given geodesic path. If one defines the geodesic starting direction by the angle (α_s) as shown in Fig. 1, then $C = -\cos \alpha_s$. The advantage of this geodesic solution lies in the fact that the integral can be quickly evaluated using numerical techniques. The important parameters of this problem are listed below:

$$z = \frac{-\cos \alpha_s}{|\sin \alpha_s|} \int_{v_i}^{v_f} \sqrt{a_f^2 \sin^2 v + b_f^2 \cos^2 v}\ dv \qquad \text{(geodesic equation)}$$

$$\ell = \frac{1}{|\sin \alpha_s|} \int_{v_i}^{v_f} \sqrt{a_f^2 \sin^2 v + b_f^2 \cos^2 v}\ dv \qquad \text{(arc length)}$$

$$\hat{e}_1 = \frac{-a_f \sin v\, \hat{x} + b_f \cos v\, \hat{y}}{\sqrt{a_f^2 \sin^2 v + b_f^2 \cos^2 v}}$$

$$\hat{e}_2 = \hat{z}$$

(curvilinear coordinates)

$$\hat{t} = \sin \alpha_s\, \hat{e}_1 - \cos \alpha_s\, \hat{e}_2$$

(unit tangent vector)

$$\hat{n} = \frac{b_f \cos v\, \hat{x} + a_f \sin v\, \hat{y}}{\sqrt{a_f^2 \sin^2 v + b_f^2 \cos^2 v}}$$

(unit normal vector)

$$\hat{b} = \hat{t} \times \hat{n} = + \cos \alpha_s\, \hat{e}_1 + \sin \alpha_s\, \hat{e}_2$$

(unit binormal vector)

$$\rho_g = \frac{(a_f^2 \sin^2 v + b_f^2 \cos^2 v)^{3/2}}{a_f\, b_f \sin^2 \alpha_s}$$

(longitudinal radius of curvature)

Using the above relations, one can employ Eqs. (1-8) to determine the total radiated fields.

These solutions were verified by a comparison with modal solutions for the limiting case of a circular cylinder as presented in Reference [3]. The solutions will be further verified by the elevation plane results presented later.

III. SCALE MODEL MEASUREMENTS

The scale model measurements presented in this report were taken at NASA (Langley, Virginia). A precise 1/25th scale model of the KC-135 aircraft was used for these measurements. Special emphasis was placed on maintaining the mount and background noise below the -30 dB level for each measured pattern. The results of this effort are well documented in the measured patterns that follow.

IV. ELEVATION PLANE RADIATION PATTERN

In most cases, the dominant structural effect in the elevation plane is the profile of the aircraft for fuselage mounted antennas. In

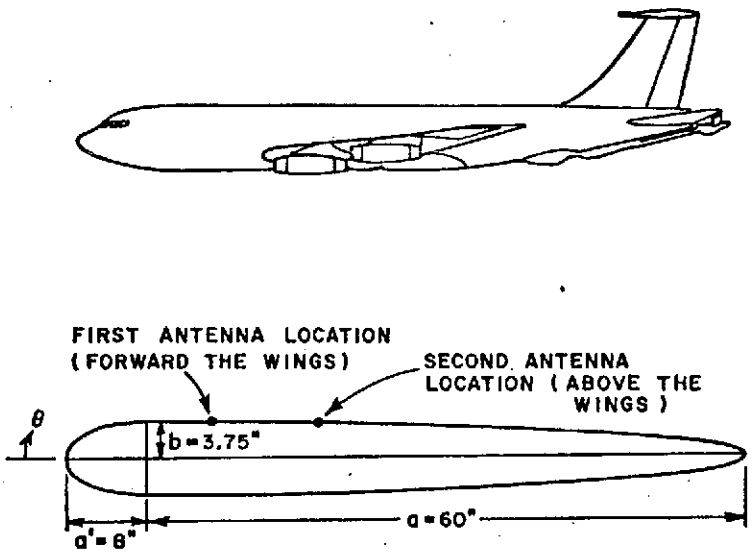

Fig. 3. Theoretical model of KC-135 aircraft.

order to simulate the wide variety of aircraft profiles, it is desirable to analyze a composite ellipse model. This model consists of two semi-ellipses mounted back-to-back.

Recall that our previous solutions are based on elliptic cylinder models; however, one of the nicer features of GTD is that it can be extended to new structures after making certain assumptions. In this case, it is assumed that there are no diffractions from the junction lines of the two ellipses. This assumption is justified since these junctions are non-existent in the actual aircraft profile. Note that the GTD solution in the lit region does not depend on the surface parameters in that it is assumed the source is mounted on an infinite ground plane tangent to the surface at the source point. On the other hand, the transition and deep-shadow region solutions are modified due to their dependence upon the surface parameters. This modification simply requires that one use $a_f=a$ for rays traveling to the right of the junction and $a_f=a'$ for rays traveling to the left of the junction. The parameters a and a' are illustrated in Fig. 3.

This model is, now, applied to analyze the elevation plane radiation patterns for antennas mounted on the KC-135 aircraft. Since the antennas of interest are located on top of the fuselage and along the center line, the most significant effects on the pattern result from the upper surface of the fuselage profile. The structure used to simulate the $1/25^{th}$ scale model consists of a 60" by 3.75" right semi-ellipse and an 8" by 3.75" left semi-ellipse.

The elevation plane patterns for a short monopole mounted forward and over the wings are illustrated in Figs. 4a and b, respectively. The patterns for a circumferential KA-band waveguide are illustrated in Figs. 5a and b. Finally, the results for an axial KA-band waveguide are shown in Figs. 6a and b. The KA-band waveguide aperture fields are simulated in our model by an array of infinitesimal elements as shown in Fig. 7.

The comparison between calculated and measured results is very encouraging especially when the antennas are located above the wings. The discrepancy displayed in the fore and aft regions particularly for the case of antennas located forward of the wing is due to the effects of the cockpit and the vertical stabilizer which are neglected in our theoretical model. However, these comparisons do show the capability of our GTD solution in determining the elevation patterns of aircraft antennas.

V. ROLL PLANE ANALYSIS

The basic aircraft to be analyzed in this study is composed of flat plates attached to infinitely long elliptic cylinders. The model was originally developed using a circular cylinder to represent the fuselage[4]. Modal solutions were used to determine the field. In the present paper, GTD solutions as presented in Section II of this paper are used to compute fields radiated from an antenna mounted on an elliptic cylinder. The basic method of solution is the same; however, a few changes must be made in the determination of the effective source location due to the difference in geometry as shown in Fig. 8.

If the source does not directly illuminate the wing, as shown in Fig. 8a, the effective source position for reflections from the right wing in terms of the radiation direction (θ_s,ϕ_s) is given by

$$
\begin{aligned}
x_e &= a_f \cos v_e \\
y_e &= b_f \sin v_e \qquad (11) \\
z_e &= \cot \theta_s \int_{v_{so}}^{v_e} \sqrt{a_f^2 \sin^2 v + b_f^2 \cos^2 v}\, dv + z_{so}
\end{aligned}
$$

where $v_e = \tan^{-1} (b_f/a_f \cot \phi_s)$. These coordinates can, then, be used in the flat plate problem as the effective source location. Note that as the desired radiation direction is varied the effective source location changes. In addition, if the source directly illuminates the wing for a given reflection term then the effective source location is simply the actual source location (u_f,v_{so},z_{so}). A result similar to Eq. (11) can be found for the reflections from the left wing.

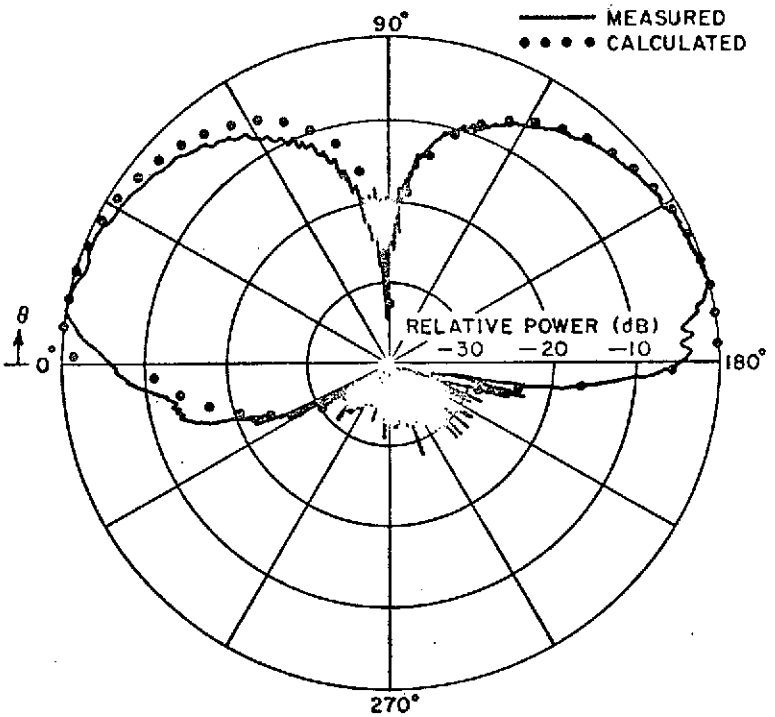

Fig. 4a. Elevation plane pattern for a λ/4 monopole mounted forward of the wings on a KC-135 aircraft.

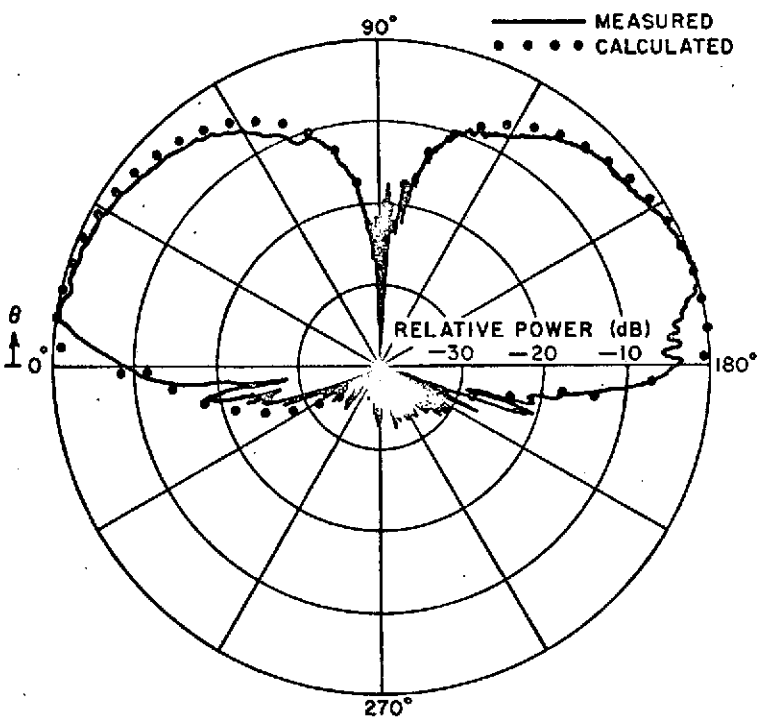

Fig. 4b. Elevation plane pattern for a λ/4 monopole mounted above the wings on a KC-135 aircraft.

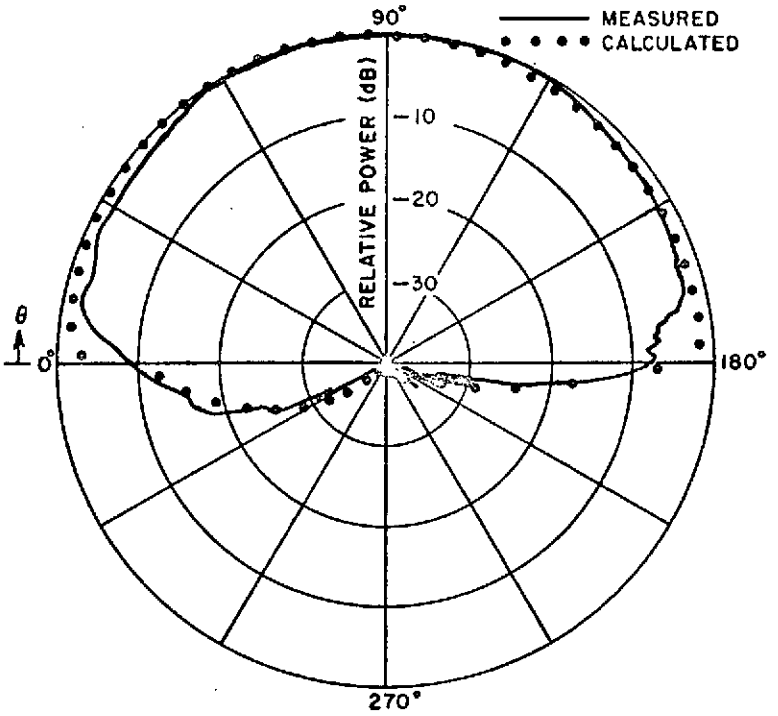

Fig. 5a. Elevation plane pattern for a circumferential KA-band waveguide mounted forward of the wings on a KC-135 aircraft.

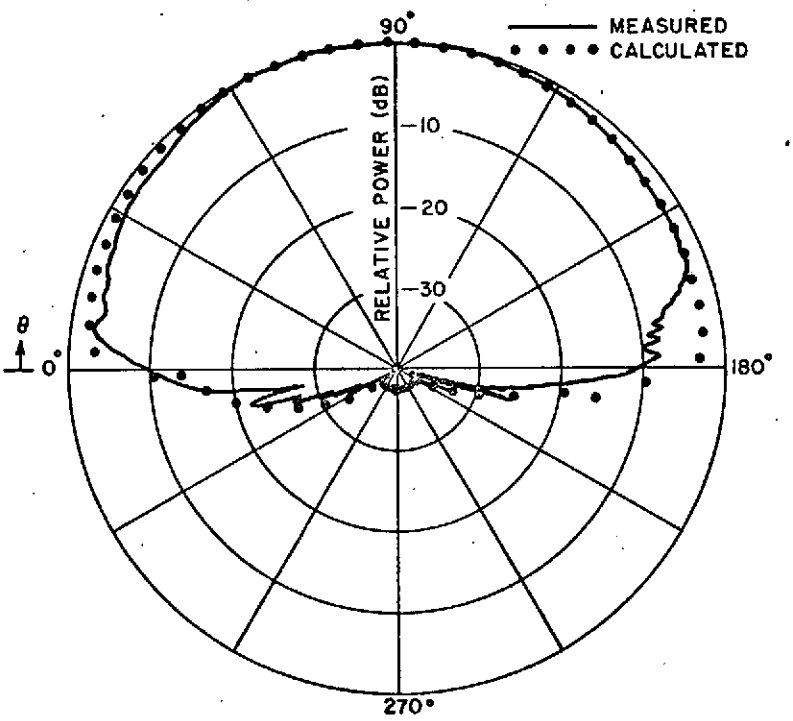

Fig. 5b. Elevation plane pattern for a circumferential KA-band waveguide mounted above the wings on a KC-135 aircraft.

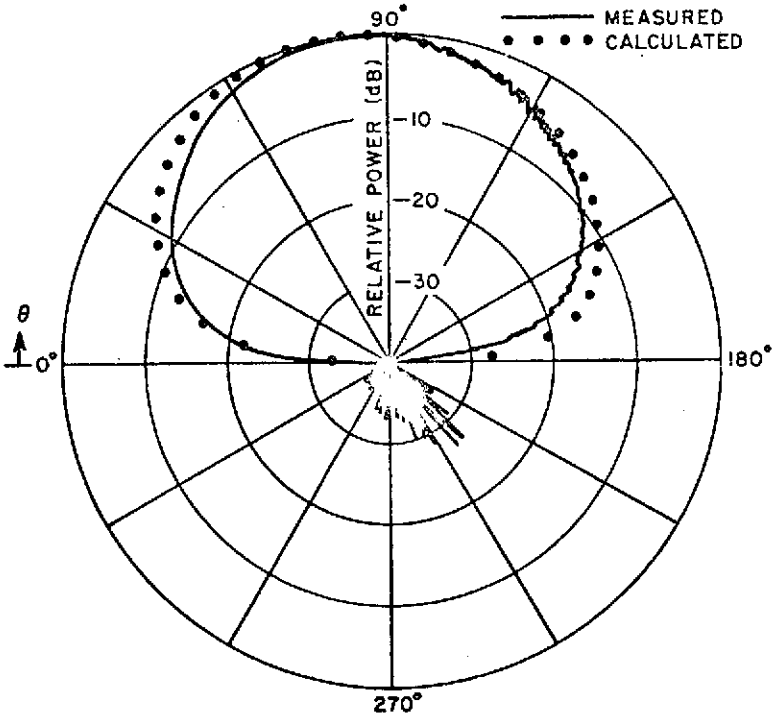

Fig. 6a. Elevation plane pattern for an axial KA-band waveguide mounted forward of the wings on a KC-135 aircraft.

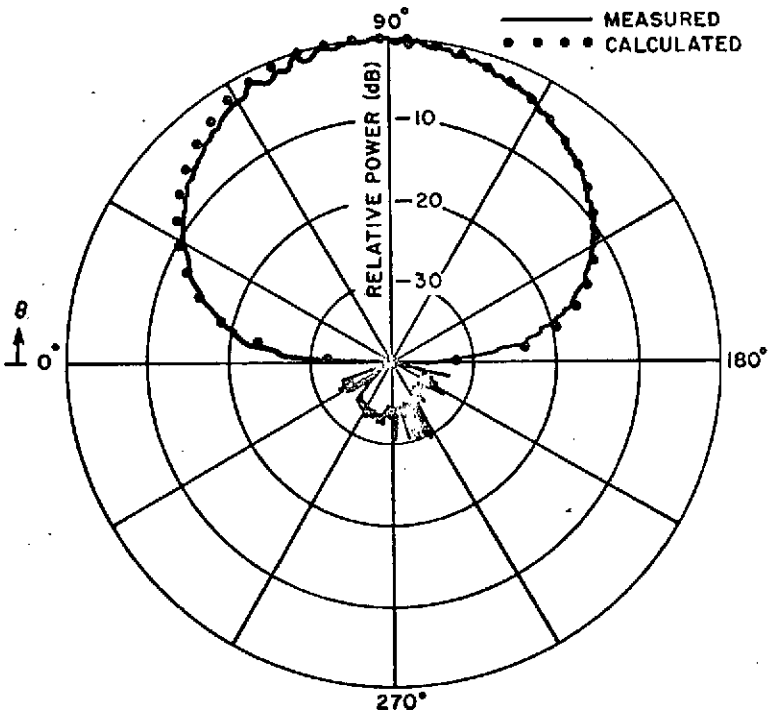

Fig. 6b. Elevation plane pattern for an axial KA-band waveguide mounted above the wings on a KC-135 aircraft.

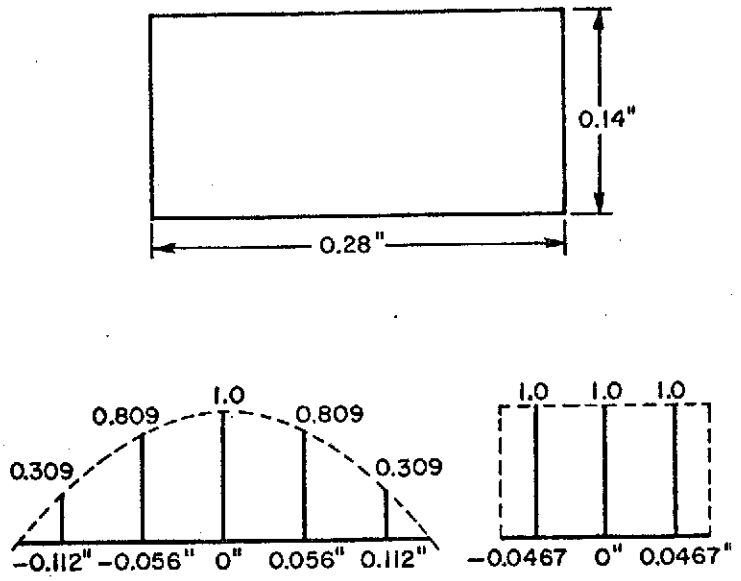

Fig. 7. Approximation of an open-end waveguide by an array of 5 infinitesimal broad wall elements with different weight and an array of 3 infinitesimal narrow wall elements with uniform weight.

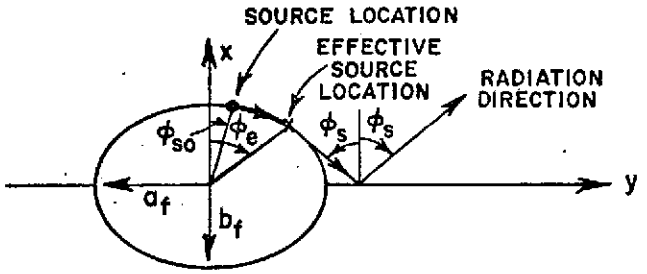

Fig. 8a. Illustration in the x-y plane of the effective source problem for reflections.

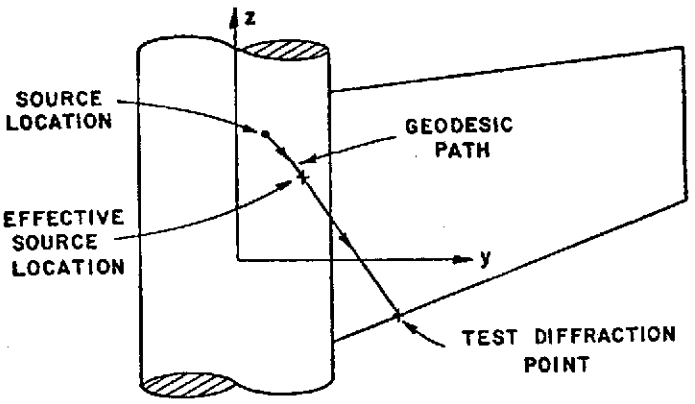

Fig. 8b. Illustration in the y-z plane of the effective source problem for edge diffractions.

Using a similar technique the effective source locations for the diffracted field components may be found. Our flat plate solution uses a search technique to find the diffraction point by computing the diffraction angles at selected test points along a given edge. Once a test point (x_d,y_d,z_d) is specified along the edge one can find the effective source location (x_e,y_e,z_e) using the geometry illustrated in Fig. 8b. Again it is assumed that the source does not directly illuminate the test point. One finds that this effective source is given by

$$x_e = \frac{a_f^2 b_f^2 x_d + a_f^2 y_d \sqrt{a_f^2 y_d^2 + b_f^2 x_d^2 - a_f^2 b_f^2}}{(a_f^2 y_d^2 + b_f^2 x_d^2)}$$

$$y_e = \frac{a_f^2 b_f^2 y_d - b_f^2 x_d \sqrt{a_f^2 y_d^2 + b_f^2 x_d^2 - a_f^2 b_f^2}}{(a_f^2 y_d^2 + b_f^2 x_d^2)} \qquad (12)$$

$$z_e = \frac{b_f x_e z_d I_v + a_f z_{so}(y_d - y_e) I_v'}{b_f x_e I_v + a_f (y_d - y_e) I_v'}$$

where

$$I_v = \int_{v_{so}}^{v_e} \sqrt{a_f^2 \sin_v^2 + b_f^2 \cos_v^2}\, dv,$$

$$I_v' = \sqrt{a_f^2 \sin^2 v_e + b_f^2 \cos^2 v_e}, \quad \text{and } v_e = \tan^{-1}\left(\frac{y_e/b_f}{x_e/a_f}\right).$$

Given the effective source location for the chosen test point, the search technique is applied to find the actual diffraction point along a given edge. Note that once the actual diffraction point is determined, the effective source of the diffracted field is specified by Eq. (12).

The results for a $\lambda/4$ monopole on the fuselage forward and over the wings are shown in Figs. 9a and b, respectively. The results for a KA-band circumferential waveguide forward and over the wings are shown in Fig. 10. The results for a KA-band axial waveguide forward and above the wings are shown in Fig. 11. The waveguide antenna is modelled as in the previous section, and the agreement in each case is very encouraging.

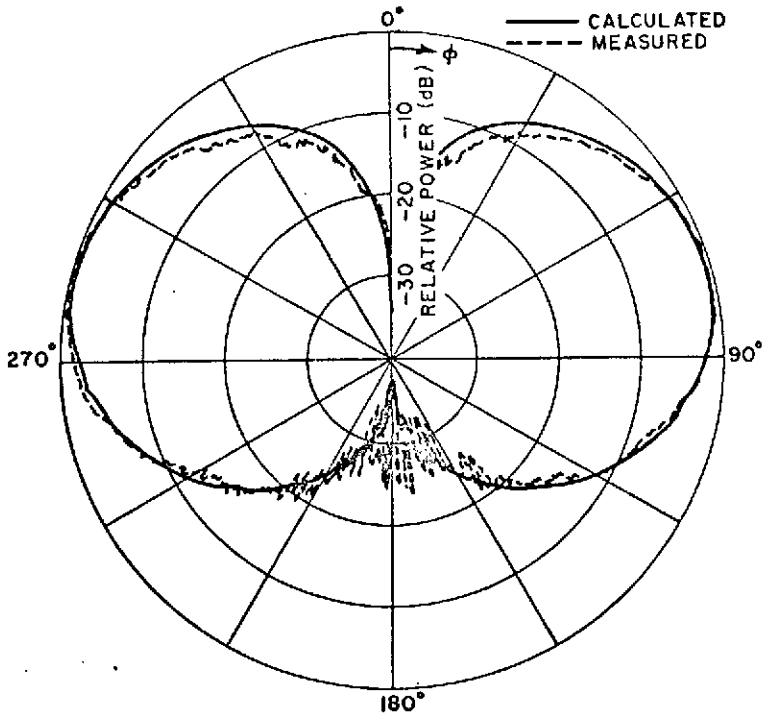

Fig. 9a. Roll plane pattern (E_ϕ) for a 1/25 scale model of a KC-135 with a $\lambda/4$ monopole on the fuselage forward of the wings at freq.=34.92 GHz (model frequency).

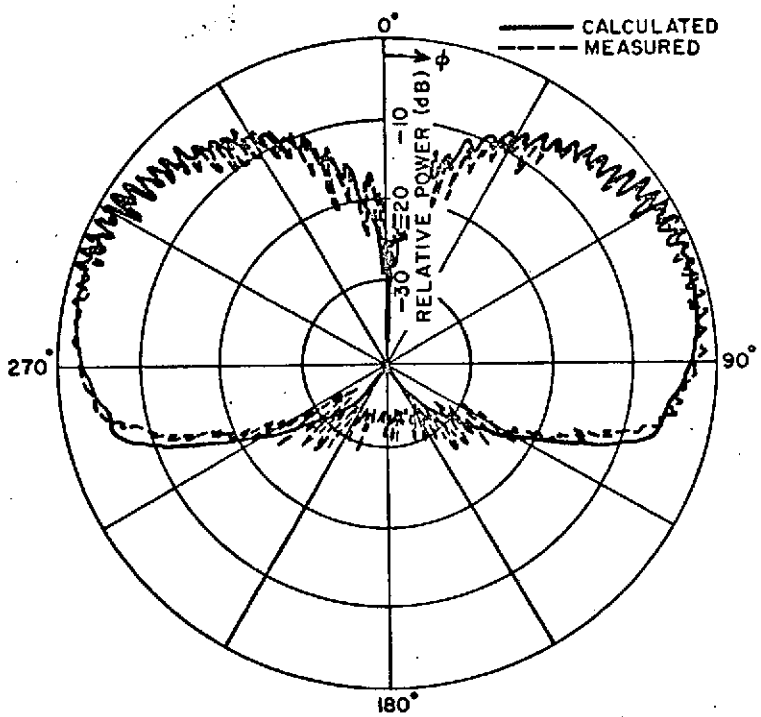

Fig. 9b. Roll plane pattern (E_ϕ) for a $\lambda/4$ monopole above the wings.

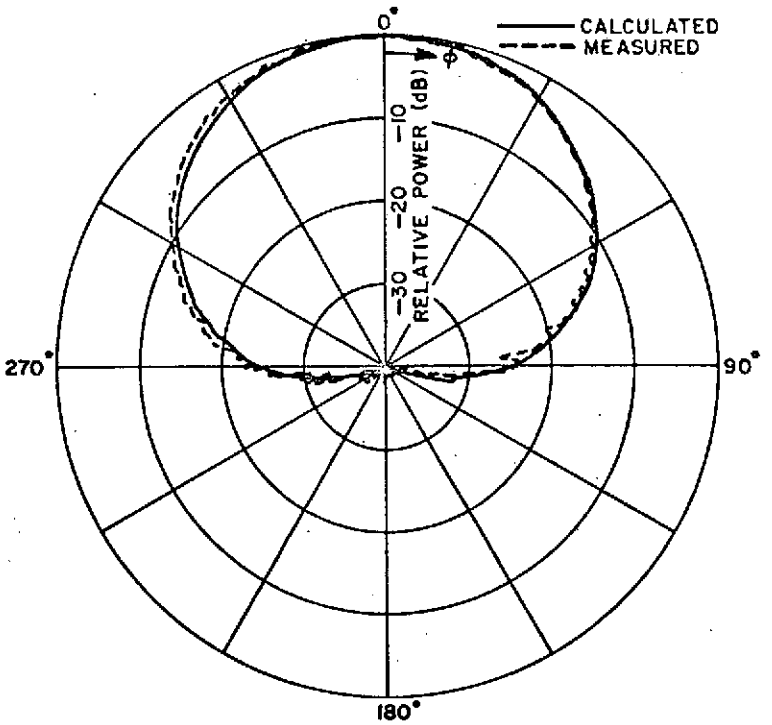

Fig. 10a. Roll plane pattern (E_θ) for a KA-band circumferential waveguide forward of the wings.

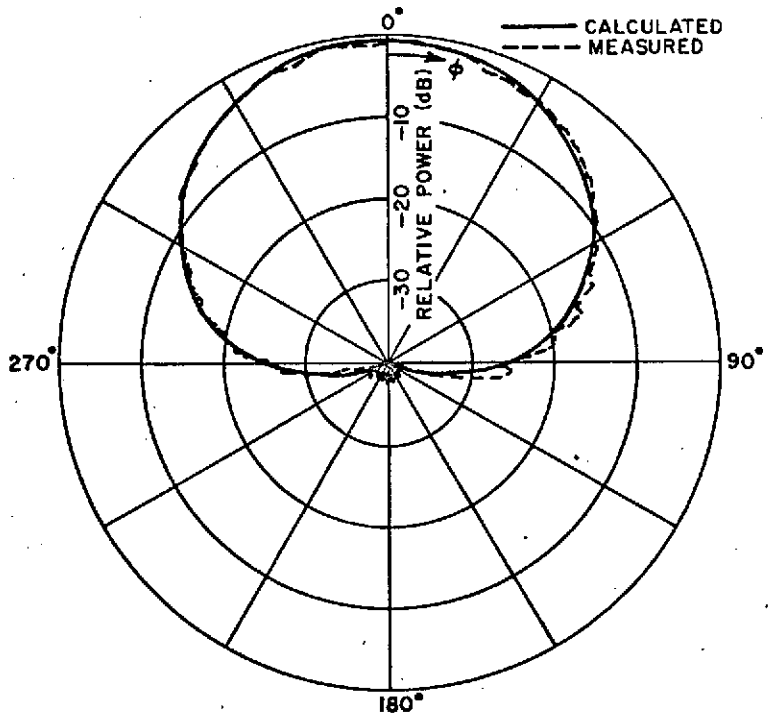

Fig. 10b. Roll plane pattern (E_θ) for a KA-band circumferential waveguide above the wings.

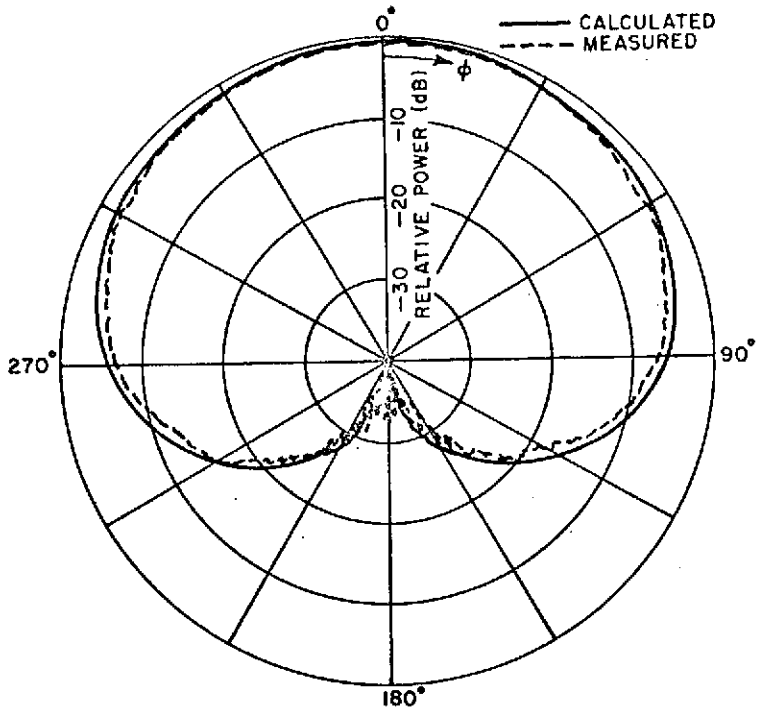

Fig. 11a. Roll plane pattern (E_ϕ) for a KA-band axial waveguide forward of the wings.

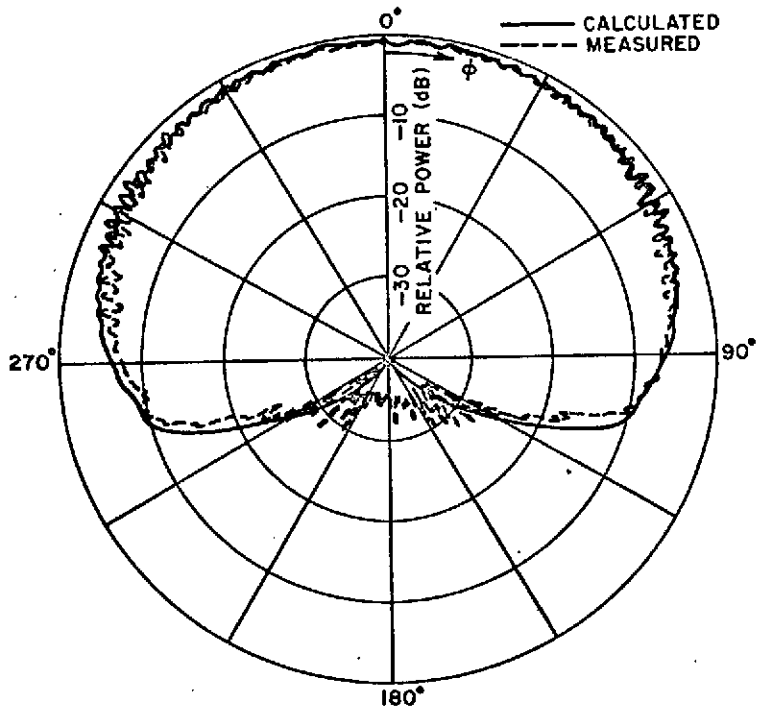

Fig. 11b. Roll plane pattern (E_ϕ) for a KA-band axial waveguide above the wings.

VI. CONCLUSIONS

The numerical solutions for the elevation and roll plane radiation patterns are developed for an antenna mounted on the fuselage of a general aircraft shape. Precision experimental results are presented for a $1/25^{th}$ scale model of a KC-135 aircraft. These results were taken at NASA (Langley, Virginia) with special emphasis on maintaining the background and mount noise below the -30 dB level. Based on the agreement between the calculated and measured results, it appears that the numerical solutions are well within engineering accuracy. In addition to the versatility already demonstrated, the roll plane solution can be applied to compute the complete volumetric pattern except for two conical sectors (fore and aft). As for efficiency both solutions run a complete pattern in approximately 30 seconds on a CDC-6600 digital computer. Consequently, a great savings can be achieved by using the computer aided model to determine the antenna design and location. Then measured patterns could be taken as a verification of the final result.

Although the solutions presented in this report are directed toward computing radiation patterns, they can also be used to compute the surface charge and current densities induced on the aircraft surface for an incident plane wave. In fact using a Fourier transform approach, one can solve for the time domain solutions for the surface charge and current densities for an incident electromagnetic pulse.

In order to complete our study of fuselage mounted antennas, one needs to examine means of handling the fore and aft sectors which cannot presently be solved using our roll plane model. The problems involved in these sectors result from the three-dimensional fuselage shape which is dominant. In addition, a model for the cockpit/radome section and vertical stabilizer effects must be developed as may be seen in the elevation plane patterns. Perhaps a model composed of a finite elliptic cylinder fuselage to which are attached flat plate wings and stabilizers (including a vertical stabilizer) is the most practical configuration. Using this model, the complete volumetric pattern can be calculated.

Another problem that is presently being considered is the effect of a moving flap on various radiation patterns. This situation is simulated by considering a stationary plate attached by a common edge to a moving plate. The moving plate can be rotated about the common edge to angle between 90° and 270°.

An aircraft/antenna problem that has not received much attention to date is that of an off-fuselage mounted antenna such as pod mounted antennas, wing mounted antennas, etc. This type of problem needs additional effort in order to develop numerical solutions comparable to the previously developed fuselage mounted antenna solutions.

REFERENCES

1. Pathak, P.H. and R.G. Kouyoumjian, "The Radiation from Apertures in Curved Surfaces," Report 3001-2, December 1972, ElectroScience Laboratory, Department of Electrical Engineering, The Ohio State University; prepared under Grant NGR 36-008-144 for National Aeronautics and Space Administration.

2. Burnside, W.D., "Analysis of On-Aircraft Antenna Patterns," Report 3390-1, August 1972, ElectroScience Laboratory, Department of Electrical Engineering, The Ohio State University; prepared under Contract N62269-72-C-0354 for Naval Air Development Center.

3. Burnside, W.D., C.L. Yu and R.J. Marhefka, "Flush-Mounted Antennas Radiating Through Dielectric-Covered Curved Surfaces," Report 3001-5, July 1973, ElectroScience Laboratory, Department of Electrical Engineering, The Ohio State University; prepared under Grant No. NGR 36-008-144 for National Aeronautics and Space Administration.

4. Burnside, W.D., R.J. Marhefka and C.L. Yu, "Roll Plane Analysis of On-Aircraft Antennas," Vol. AP-21, No. 6, November 1973, pp. 780-786.